EVOLUTION OF MALE COLORATION DURING A POST-PLEISTOCENE RADIATION OF BAHAMAS MOSQUITOFISH (*GAMBUSIA HUBBSI*)

Ryan A. Martin[1,*], Rüdiger Riesch[2], Justa L. Heinen-Kay, and R. Brian Langerhans

SUPPLEMENTAL MATERIAL A: SEXUAL DIMORPHISM IN BODY COLOR, SIZE, AND SHAPE

METHODS

Traits evaluated in this study were chosen because they have the appearance of conspicuous signals. Secondary sexual traits important in conspecific signaling often exhibit sexual dimorphism (Andersson 1994), thus we wished to assess the degree of sexual dimorphism for each color trait examined in this study. We tested for sexual dimorphism by comparing coloration traits of adult males and females from two high-predation (Cousteau's and West Twin) and two low-predation (Hubcap and East Twin) blue holes (see Fig. SB1 for location of sites).

Male coloration was measured as described in the Methods. We collected 6-12 mature female *G. hubbsi* using hand-held dip nets and minnow traps from the four populations listed above—previously used for the measurement of male coloration—during a single week in June 2011. We took each photograph with a Canon G12 digital camera, and measured coloration using Adobe Photoshop CS5.1 following the detailed methods described in Supplemental Material B. We did not measure female anal fin a^* or b^* coloration because a preliminary visual survey suggested that female anal fins completely lack red and yellow coloration.

We then tested if each trait was sexually dimorphic, and if male and female traits responded similarly across predation regime. To do this we ran separate linear mixed models for each trait. In each model we included log-transformed standard length (SL) as a covariate, and predation regime, sex and the interaction between predation regime and sex as independent variables. We also included population as a random intercept fit using restricted maximum likelihood (REML). Using just the data collected from females, we additionally asked if predation regime explained variation in female coloration for each trait among blue holes again using separate linear mixed models for each trait. In each model we included log-transformed SL as a covariate, predation regime as the independent variable, and population as a random intercept fit using REML. In all cases we employed the Kenward–Roger degrees of freedom adjustment (Kenward and Rogers 1997) for significance testing.

To further illustrate the generality of sexual dimorphism in *G. hubbsi*, we also present data on sexual dimorphism in body size and shape using morphometric data extracted from Riesch et al. (Submitted ms.), and measured using established and previously described methods (e.g., see Langerhans et al. 2004, 2007).

RESULTS

Five of six measured traits were sexually dimorphic (Table SA1). Controlling for effects of body size, males had more red ($\uparrow a^*$) and yellow ($\uparrow b^*$) dorsal-fin coloration, larger iridescence patch, and darker caudal-fin pigmentation (Fig. SA1). In addition we found that males possessed relatively larger black shoulder patches than females in low-predation, but not high-predation sites (Fig. SA1-E). The only trait that did not exhibit sexual dimorphism was gonopodium / anal-fin blackness, suggesting that this may not represent a sexual signal—although, because this fin

size and shape is highly sexually dimorphic, and female preferences for gonopodium size is known for multiple species (e.g., Langerhans et al. 2005; Kahn et al. 2010), this requires further study. Finally, female body coloration did not differ across predation regimes (Table SA2). Patterns of sexual dimorphism in body size (Table SA3) and shape (Figure SA2) are presented below.

Table SA1. Summary of results from linear mixed models testing for sexual dimorphism in *Gambusia hubbsi* body color.

Trait	Parameter	*DF*	*F*	*P*
Dorsal fin *a**	log SL	1,66.02	5.10	0.028
	Pred	1,2.08	1.23	0.379
	Sex	1,65.19	62.91	<0.001
	Pred x Sex	1,65.10	1.830	0.181
Dorsal fin *b**	log SL	1,65.55	1.22	0.274
	Pred	1,2.01	0.11	0.773
	Sex	1,65.07	203.78	<0.001
	Pred x Sex	1,65.02	1.411	0.239
log Iridescence	log SL	1,71.98	20.73	<0.001
	Pred	1,2.14	0.27	0.654
	Sex	1,70.52	32.92	<0.001
	Pred x Sex	1,70.52	0.24	0.626
log Black shoulder patch	log SL	1,48.73	7.89	0.007
	Pred	1,2.623	0.287	0.634
	Sex	1,67.37	0.00	0.989
	Pred x Sex	1,66.59	11.00	0.002
Caudal fin *L**	log SL	1,38.95	8.63	0.006
	Pred	1,1.80	1.40	0.370
	Sex	1,69.07	24.20	<0.001
	Pred x Sex	1,69.48	3.26	0.075
Anal fin / gonopodium *L**	log SL	1,69.74	3.09	0.083
	Pred	1,2.10	0.44	0.571
	Sex	1,68.43	0.23	0.635
	Pred x Sex	1,68.32	0.13	0.722

Table SA2. Summary of results from linear mixed models testing for divergence in female *Gambusia hubbsi* body color between high and low predation blue holes.

Trait	Parameter	*DF*	*F*	*P*
Dorsal fin *a**	log SL	1,27	0.428	0.518
	Pred	1,2	0.346	0.615
Dorsal fin *b**	log SL	1,27	0.428	0.518
	Pred	1,2	0.346	0.615
log Iridescence	log SL	1,32	7.299	0.011
	Pred	1,2	0.002	0.963
log Black shoulder patch	log SL	1,28	14.899	0.001
	Pred	1,2	4.513	0.167
Caudal fin *L**	log SL	1,30	9.883	0.003
	Pred	1,2	1.851	0.306
Anal fin *L**	log SL	1,31	2.141	0.153
	Pred	1,2	0.167	0.722

Table SA3. Summary of sex differences in body size in *Gambusia hubbsi* inhabiting blue holes (data from Riesch et al. 2013).

		Female Standard Length (mm)			Male Standard Length (mm)		
Predation Regime	Population	N	Mean	Std. Dev.	N	Mean	Std. Dev.
Low	East Twin	11	30.35	3.94	10	22.72	2.32
Low	Gollum's	11	30.14	3.49	10	24.50	2.19
Low	Hubcap	19	24.64	1.62	10	22.28	2.61
Low	Ken's	28	30.09	2.83	10	24.62	2.34
Low	Pigskin	21	27.94	4.33	10	22.08	3.43
Low	Rainbow	26	26.33	2.45	10	23.37	2.21
Low	Voy's	10	28.40	3.67	10	20.68	2.29
High	Cousteau's	9	35.29	2.82	10	24.70	1.94
High	Hard Mile	9	28.06	3.89	10	22.18	1.45
High	Rivean's	5	29.84	3.44	10	23.97	2.85
High	Runway	7	25.04	2.07	10	22.65	2.19
High	Shawn's	22	26.93	4.52	10	20.50	2.91
High	Stalactite	10	30.36	1.92	10	22.80	2.30
High	West Twin	10	27.95	2.17	10	23.61	1.75

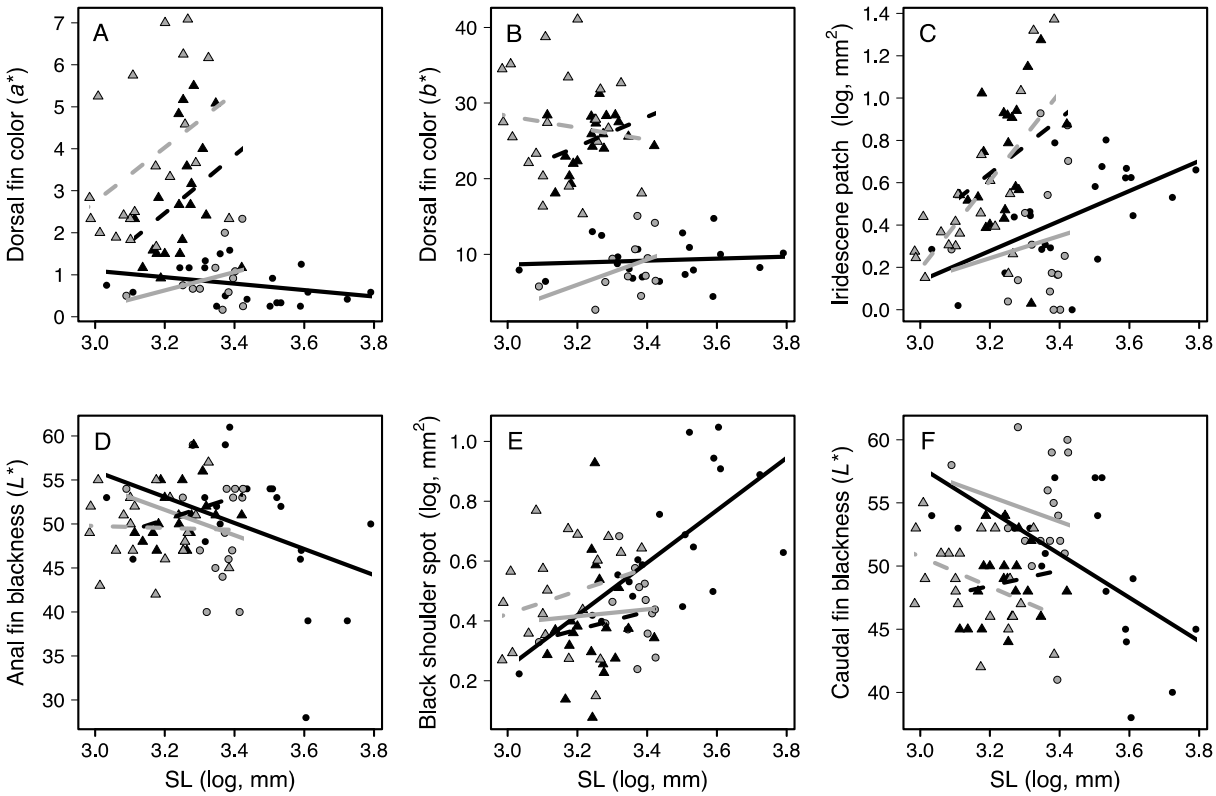

Figure SA1. The relationship between body color traits and standard length (SL) for male (triangle symbols and dashed lines) and female (filled circles and solid lines) *Gambusia hubbsi* in low-predation (grey symbols and lines) and high-predation (black symbols and lines) blue holes.

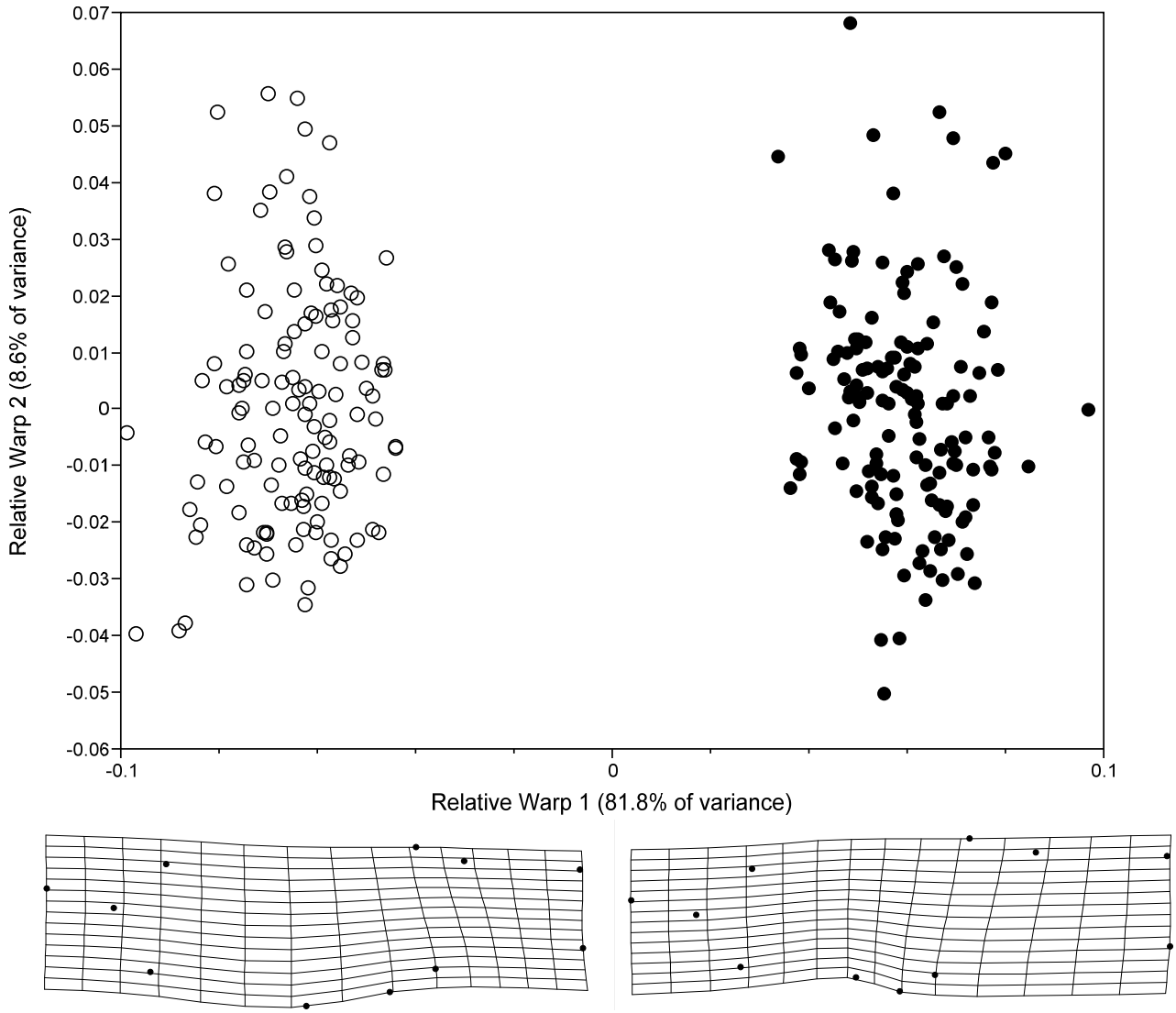

Figure SA2. Illustration of strong sexual dimorphism in body shape in *Gambusia hubbsi* (open circles: females, filled circles: males; data from Riesch et al. Submitted ms.). Thin-plate spline transformation grids illustrate variation associated with negative and positive scores along RW1.

Literature Cited

Andersson, M. B. 1994. Sexual selection. Princeton University Press, Princeton, NJ.

Kahn, A. T., B. Mautz and M. D. Jennions. 2010. Females prefer to associate with males with longer intromittent organs in mosquitofish. Biol. Lett. 6:55-58.

Kenward, M. G. and J. H. Roger. 1997. Small sample inference for fixed effects from restricted maximum likelihood. Biometrics 53:983–997.

Langerhans, R. B., C. A. Layman and T. J. DeWitt. 2005. Male genital size reflects a tradeoff between attracting mates and avoiding predators in two live-bearing fish species. Proc. Natl. Acad. Sci. USA 102:7618-7623.

Langerhans, R. B., M. E. Gifford and E. O. Joseph. 2007. Ecological speciation in gambusia fishes. Evolution 61:2056–2074.

Langerhans, R. B., C. A. Layman, A. M. Shokrollahi and T. J. DeWitt. 2004. Predator-driven phenotypic diversification in *Gambusia affinis*. Evolution 58:2305–2318.

Riesch, R., Martin R. A., and Langerhans R. B. 2013 Predation's role in life-history evolution of a livebearing fish and a test of the Trexler-DeAngelis model of maternal provisioning. Am. Nat. 181:78–93.

EVOLUTION OF MALE COLORATION DURING A POST-PLEISTOCENE RADIATION OF BAHAMAS MOSQUITOFISH (*GAMBUSIA HUBBSI*)

Ryan A. Martin[1,*], Rüdiger Riesch[2], Justa L. Heinen-Kay, and R. Brian Langerhans

SUPPLEMENTAL MATERIAL B: ADDITIONAL METHODOLOGICAL DETAILS

- **LOCATION OF STUDY SITES**
- **PHOTOGRAPHIC METHODS**
- **ENVIRONMENTAL MEASUREMENTS**
- **MORPHOLOGICAL DIVERGENCE**
- **POPULATION GENETIC ANALYSIS**
- **COMMON-GARDEN EXPERIMENT**
- **RELATIONSHIPS BETWEEN COLOR TRAITS AND ENVIRONMENTAL FACTORS AND CONDITION**

Location of Study Sites

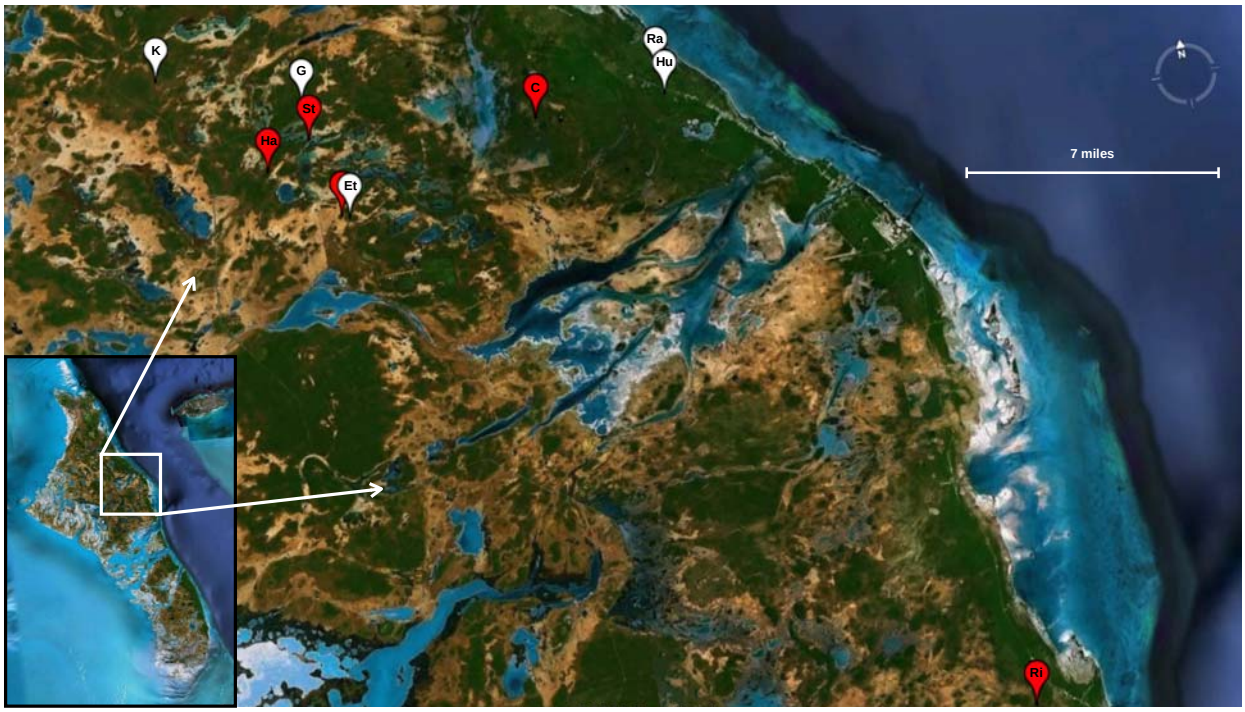

Figure SB1. Overview of the study area on northern Andros Island, The Bahamas (inset) with locations of all sampled blue holes. Low-predation sites in white: Gollum's (G), East Twin (ET), Hubcap (Hu), Ken's (K), Rainbow (Ra). High-predation sites in red: Cousteau's (C), Hard Mile (Ha), Rivean's (Ri), Stalactite (St), West Twin (hidden behind white ET). Maps were created with Google Earth.

Photographic Methods

Immediately after capture we used a Canon G12 digital camera to take individual photographs of each male inside a portable photo studio comprising a matte-black lined box, allowing constant lighting conditions for each image (identical flash intensity, aperture, shutter speed). We placed

live specimens laterally on a white background, splayed the dorsal and caudal fins, and positioned the gonopodium laterally and approximately perpendicular to the body anteroposterior axis (Fig. SB2). We placed color standards (24-color color checker), a greyscale and a ruler beside each specimen. We saved images in RAW format to avoid loss of information from file compression (Stevens et al. 2007). Prior to color measurement, we manually white-balanced images using the white color standard in each image and converted each file to a 16-bit TIFF in Adobe Photoshop CS5.1. We evaluated the response of the camera's RGB output to light intensity by plotting the measured RGB values of the greyscale in each image against the color standards' known values. No corrections were necessary because the camera's outputs were linear and equal across the RGB channels (Stevens et al. 2007).

Environmental Measurements

We measured near-shore habitat color and water color using underwater digital photography (same camera as above). Placement of photographs within blue holes was selected based on the typical location of *G. hubbsi* within these sites (Heinen et al. 2013), and so as to avoid effects of differential penetration of light wavelengths with increasing depth. To measure habitat color at each blue hole we used images taken horizontally to the water column, facing toward the shore/wall at an average depth of 0.5 m, and an average distance of 0.5 m (shores of most blue holes are very steep, and thus horizontal photographs capture background colors of the near-vertical walls). All images contained a white color standard card placed beside the substrate. We saved RAW image files, manually white-balanced each image using the white color standard, and then converted each image to a 16-bit TIFF for analysis as described in the main text (see Methods). For each of three images per blue hole, we sampled the average a^* and b^* color values from five randomly chosen, 9 x 9 pixel squares. We calculated the average a^* and b^* values for each image and then calculated averages across all three images for each site. We reduced dimensionality by conducting a PCA on the correlation matrix of the a^* and b^* average values. We retained all PC axes that explained more variation that that expected under a broken-stick model (Frontier 1976; Jackson 1993). This resulted in retention of one PC axis. Larger values along this PC axis correspond with higher a^* and b^* values (see Supplementary Material C).

We measured water color at each blue hole using methods similar to that for habitat color, with the exceptions that images were taken facing outward from the shore, a single randomly chosen 9 x 9 pixel square was examined for each of two images from each blue hole (considerably less variance was observed for water color than habitat color see Fig. SB2), and we did not use PCA in this case because values at one site drove a spurious negative covariance between the a^* and b^* values.

To estimate relative algal biomass we measured the photosynthetic pigment chlorophyll *a* using a fluorometer (AquaFluor model, Turner Designs, Sunnyvale, CA). Zooplankton densities were estimated using a 60-m tow of a zooplankton net (20-cm diameter, 153-µm mesh) at 0.5-m depth. All zooplankton were counted within a 2.5-ml subsample of each plankton collection using a stereo microscope. Further details provided in Heinen et al. (2013).

At the time of fish sampling, we measured tertiary (adult) sex ratio of *G. hubbsi*— calculated as the density of females divided by the density of males—using underwater visual census methods (English et al. 1994; Nagelkerken et al. 2000; Heinen et al. 2013). Briefly, while snorkeling, one author (RBL) recorded the number of mature male and female *G. hubbsi* present in 1-m^3 quadrats within each of four habitat types: (1) shallow near-shore (0-1 m deep, 1-2 m from shore), (2) deep near-shore (2-3 m deep, 1-2 m from shore), (3) shallow offshore (0-1 m

deep, 9-10 m from shore), and (4) deep offshore (2-3 m deep, 9-10 m from shore). Counts were made immediately upon arrival within a 1-m distance of the pre-designated quadrat location to avoid disturbing the fish. We surveyed 10 quadrats within each habitat type distributed equidistant around the perimeter of each blue hole (repeatability of *G. hubbsi* density across time of day, seasons, and years supports the use of these snapshot estimates, Heinen et al. 2013). Overall average densities of each sex were calculated across all habitat types.

Figure SB2. Representative background water color and corresponding *a** and *b** color values (top) and representative male *G. hubbsi* (bottom) from each study site (top panel: low-predation sites; bottom panel: high-predation sites). Neither water color (*a**: $F = 2.455$, $P = 0.156$; *b**: $F = 0.225$, $P = 0.648$) nor background habitat color (PC1 of habitat color (not shown): $F = 0.649$, $P = 0.444$) significantly differed between predation regimes.

Morphological Divergence

Using tpsRelw (Rohlf 2010), we performed generalized Procrustes analysis (i.e., aligned landmark coordinates by rotating, translating and scaling coordinates to remove positioning effects and isometric size effects; Bookstein 1991; Marcus et al. 1996) on 17 landmarks: (1) most anterodorsal point of premaxilla, (2) indentation at the posterodorsal end of premaxilla, (3) indentation at the posterodorsal end of head, (4) anterior insertion of dorsal fin, (5) posterior insertion of dorsal fin, (6) dorsal insertion of caudal fin, (7) posterior tip of hypural plate, (8) ventral insertion of caudal fin, (9) posterior insertion of anal fin, (10) anterior insertion of anal fin, (11) intersection of the operculum and ventral body profile, (12) indentation near the posteroventral end of lower jaw, (13) anterior edge of eye, (14) center of eye, (15) posterior edge of eye, (16) dorsal insertion of pectoral fin, and (17) ventral insertion of pectoral fin (see Fig. 2 in main text). We obtained shape variables (partial warps and uniform components) in tpsRelw for statistical analysis. To confirm previously reported predator-driven body-shape divergence, we tested for differences between predation regimes using a mixed-model MANCOVA (see Riesch et al. 2013); we then calculated a divergence vector (**d**) from the predation regime term of this model following Langerhans (2009), which describes the multivariate axis exhibiting the greatest difference between predation regimes without scaling differences to within-group (co)variation (statistically controlling for allometry). Results confirmed previous findings (deeper mid-body / caudal region and smaller head in high-predation populations; see Fig. SB3).

This divergence vector was used in subsequent analyses as an estimate of multivariate body shape, capturing the aspects of body shape most influenced by the presence and absence of fish predators.

For median fin sizes, we measured two components of each fin: dorsal fin length (distance between landmarks 4 and 5) and height (distance from landmark 4 to distal tip of ray 2); gonopodium length (distance from landmark 10 to distal tip of gonopodium) and area (traced outline of gonopodium); and caudal-fin length (distance from landmark 7 to posterior tip of caudal fin) and height (maximum dorsoventral length of splayed caudal fin). We performed PCA on each set of two variables using the correlation matrix, and used the first PC axis for each fin in analyses described in the main text.

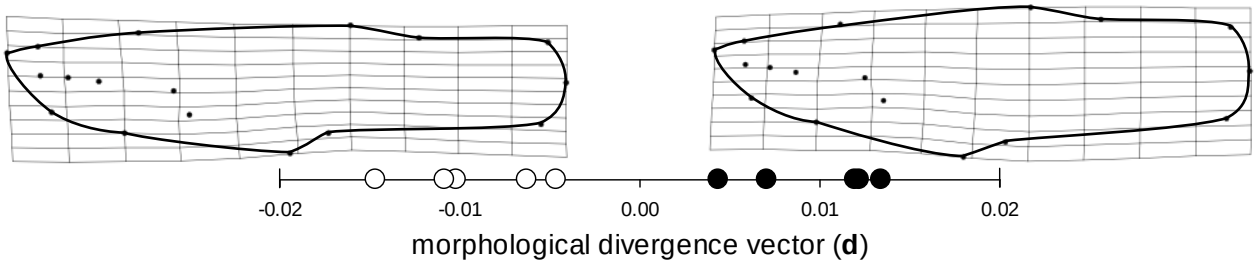

Fig. SB3 Thin-plate spline transformation grids illustrating morphological divergence between predation regimes in male *G. hubbsi* inhabiting blue holes on Andros Island, The Bahamas based on analysis of 115 males from 10 blue holes included in this study (observed variation depicted along **d**, lines drawn to aid interpretation). MANCOVA revealed strongly divergent morphologies between predation regimes ($P < 0.001$), consistent with previous work. Population means presented along **d**.

Population Genetic Analysis

To examine population genetic structure and confirm earlier results that populations within predation regimes are not more closely related to one another than to populations in the alternative predation regime (Langerhans 2007; Riesch et al. 2013) we examined published sequences of a 886bp fragment of the NADH subunit 2 (ND2) mitochondrial gene for five *G. hubbsi* individuals from each of the populations studied here (see GenBank accession numbers in Langerhans et al. 2007, Riesch et al. 2013). We then conducted an analysis of molecular variance (AMOVA) testing for three sources of molecular genetic variance: between predation regimes, among populations within predation regimes, and within populations. We found strong population genetic structure, consistent with colonization of blue holes 1000s of years ago with minimal gene flow ever since. Moreover, we found strong evidence that genetic relatedness is not associated with predation regime (Table SB1). In addition, we tested for associations between male coloration and genetic relatedness, as well as male coloration and geographic distance (straight-line distance) using separate Mantel tests (Mantel 1967). Pairwise population differences in male coloration were estimated using Mahalanobis distance based on all eight color variables (see Fig. 2). Mean genetic distance between populations was estimated as the pairwise uncorrected percent nucleotide differences (*p*-distance) using the ND2 mtDNA gene (Table SB1). Results from these separate Mantel tests found no support for an association between male coloration and genetic relatedness (one tailed $P = 0.50$), or male coloration and geographic distance (one tailed $P = 0.76$).

Table SB1. Analysis of molecular variance (AMOVA) based on mtDNA. F_{CT} is the correlation for random pairs of haplotypes within a predator regime, relative to that of random pairs of haplotypes drawn from the whole system. F_{SC} is the correlation for random pairs of haplotypes within populations, relative to that of random pairs of haplotypes drawn from the same predator regime. F_{ST} is the correlation for random pairs of haplotypes within populations, relative to that of random pairs of haplotypes drawn from the whole system.

Source of variation	*DF*	% of variation	*F*-statistic	*P*
Among predator regimes	1	0.13	FCT = 0.001	0.420
Among populations within predator regimes	8	70.31	FSC = 0.70	< 0.001
Within populations	40	29.56	FST = 0.70	< 0.001
Total	49			

Common-garden Experiment

We measured dorsal-fin color for (1) wild-caught males held under common conditions for 8-13 months, and (2) lab-born offspring raised to sexual maturity under the same common conditions (Table SB2). Because of low statistical power in these analyses, this experiment serves as a first step in assessing the genetic basis of dorsal-fin color divergence—while we can have confidence in significant effects, non-significant effects should be treated more cautiously and await further research. The primary goal of this experiment was to rule out dietary effects as the dominant explanation for differences between predation regimes, and our experimental design should be capable of accomplishing this goal. That is, males derived from different predation regimes should exhibit similar color values after receiving a common diet in the lab if diet served as the primary agent underlying color differences observed between predation regimes in the wild.

Table SB2. Sample sizes for males examined in the common-garden experiment.

Population	Predation regime	Wild caught Lab diet	Lab born F1 Lab diet	Lab born F2 Lab diet
East Twin	Low predation	5	1	0
Gollum's	Low predation	1	1	5
Cousteau's	High predation	5	4	0
Stalactite	High predation	5	2	6

Male body color, environmental factors, and individual body condition

For the four color variables where differences between predation regimes were evident based on model selection results, other factors included in the models were additionally important. In Fig. SB4, we illustrate the effects of both predation regime and an additional environmental factor or individual condition variable that significantly influenced each trait.

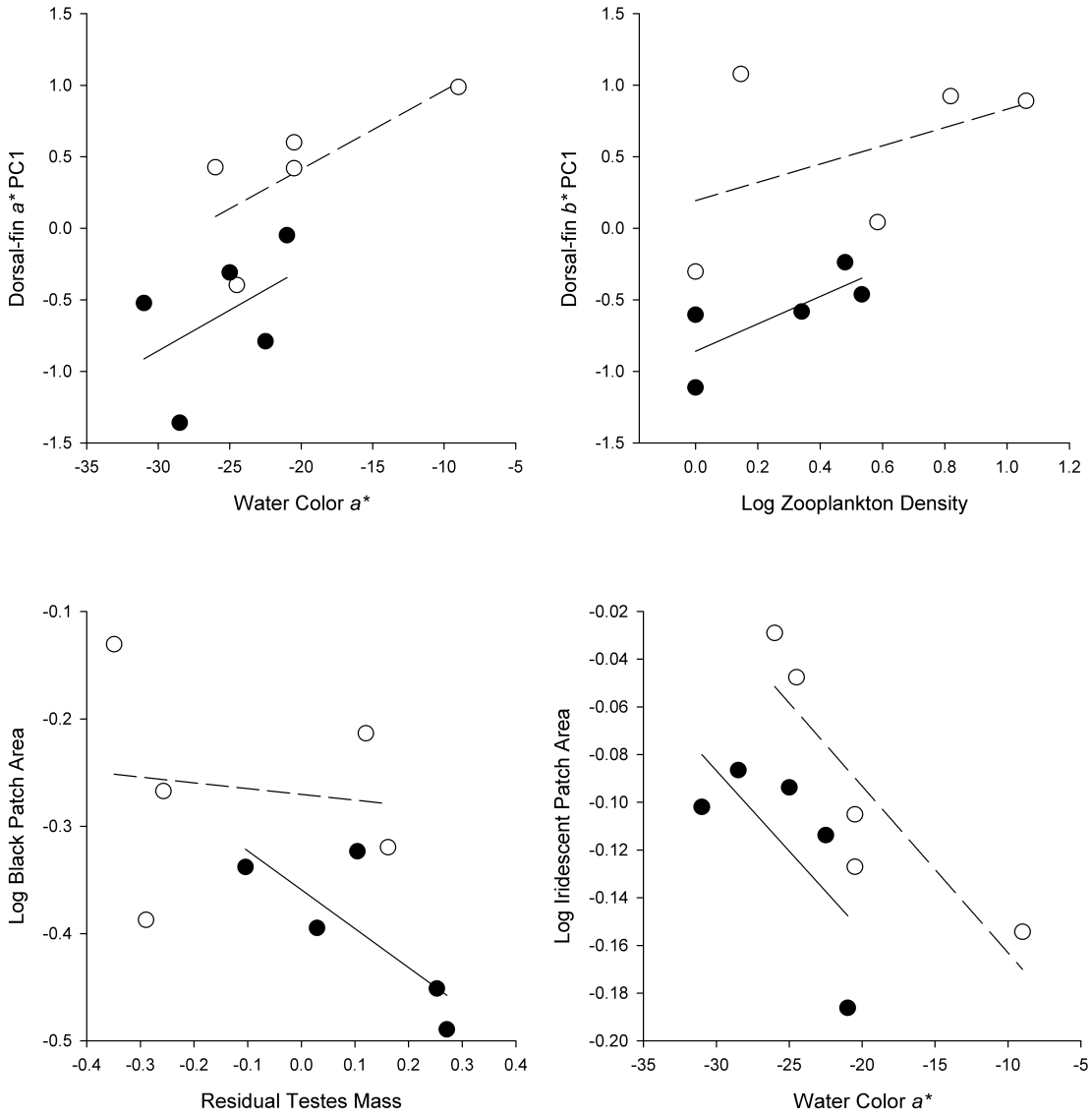

Fig. SB4 Relationships between population means for four body color variables and environmental variation / individual condition for male *Gambusia hubbsi* in low-predation (open symbols and dashed lines) and high-predation (filled symbols and solid lines) blue holes.

Literature Cited

Bookstein, F. L. 1991. Morphometric tools for landmark data: geometry and biology. Cambridge Univ. Press, UK.

English, S., C. Wilkinson and V. Baker (eds). 1994. Survey Manual for Tropical Marine Resources. *in* ASEAN-Australian Marine Science Project: Living Coastal Resources. Aus. Inst. Mar. Sci., Townsville.

Frontier, S. 1976. Étude de la décroissance des valeurs propres dans une analyse en composantes principales: Comparaison avec le modd́le du bâton brisé. J. Exp. Mar. Biol. Ecol. 25:67–75.

Heinen, J. L., M.W. Coco, M. S. Marcuard, D. N. White, M. N. Peterson, R. A. Martin and R. B.

Langerhans. 2013. Environmental drivers of demographics, habitat use, and behavior during a post-Pleistocene radiation of Bahamas mosquitofish (*Gambusia hubbsi*). Evol. Ecol. (in press).
Jackson, D. A. 1993. Stopping Rules in Principal Components Analysis: A Comparison of Huristical and Statistical Approaches. Ecology 74:2204–2214.
Langerhans, R. B., M. E. Gifford and E. O. Joseph. 2007. Ecological speciation in *Gambusia* fishes. Evolution 61:2056–2074.
Langerhans, R. B. 2009. Trade-off between steady and unsteady swimming underlies predator-driven divergence in *Gambusia affinis*. J. Evol. Biol 22:1057–1075.
Mantel, N. 1967. The detection of disease clustering and a generalized regression approach. Cancer Res. 27:209–220.
Marcus, L. F., M. Corti, A. Loy, G. J. P. Naylor and D. E. Slice. 1996. Advances in morphometrics. Springer.
Nagelkerken, I., G. van der Velde, M. W. Gorissen, G. J. Meijer, T. Van't Hof and C. den Hartog. 2000. Importance of Mangroves, Seagrass Beds and the Shallow Coral Reef as a Nursery for Important Coral Reef Fishes, Using a Visual Census Technique. Estuarine Coastal Shelf Sci. 51:31–44.
Riesch, R., R. A. Martin, and R. B. Langerhans. 2013. Predation's role in life-history evolution of a livebearing fish and a test of the Trexler-DeAngelis model of maternal provisioning. Am. Nat. 181:78–93.
Rohlf, F. J. 2010. TpsDig. Department of Ecology and Evolution, State Univ. New York, Stony Brook
Stevens, M., C. A. Párraga, I. C. Cuthill, J. C. Partridge and T. S. Troscianko. 2007. Using digital photography to study animal coloration. Biol. J. Linn. Soc. 90:211–237.

EVOLUTION OF MALE COLORATION DURING A POST-PLEISTOCENE RADIATION OF BAHAMAS MOSQUITOFISH (*GAMBUSIA HUBBSI*)

Ryan A. Martin[1,*], Rüdiger Riesch[2], Justa L. Heinen-Kay, and R. Brian Langerhans

SUPPLEMENTAL MATERIAL C: ALTERNATIVE ANALYSIS OF MALE DORSAL- AND ANAL-FIN COLOR

Our goal in this study was to investigate the factors underlying male *Gambusia hubbsi* body color variation; exploring how *G. hubbsi* and *Gobiomorus dormitor* perceive this color variation is a topic that should be explored in future studies. Because human-derived color spaces, such as the Commission Internationale de l'Éclairage (CIE) Laboratory color space, do not accurately describe how non-human species perceive color, we additionally analyzed our fin-color data (*a** and *b** channel information for dorsal and anal fins) using species-independent measures of color variation to ensure that our results were robust across particular choices of color space.

METHODS

For cases in the text where we examined if variation in the *a** and *b** values from the CIE *L*a*b** color space (dorsal- and anal-fin coloration) significantly differed between predation regimes, we additionally employed an alternative method described by Endler (2012) to quantify color variation using a color space independent of the visual system of the viewer. First, we used the same methods and images described in the Methods and Supplemental Material B with the exception that we measured dorsal- and anal-fin RGB color values rather than *L*a*b** color values. We then calculated two visual-system independent color channels from the RGB values using the equations (R-G)/(R + G) and (G-B)/(G + B) (Endler 2012; McKay 2013).

Male coloration in wild-caught males across blue holes

For wild-caught males across the 10 blue holes, we reduced the dimensionality of our dorsal- and anal-fin color metrics by performing a PCA separately for the R:G and G:B color channels for each fin, using the same methods as described in the Statistical Analyses. We retained PC axes that explained more variation than expected under a broken-stick model, resulting in a single PC axis for each color channel for each fin (Frontier 1976; Jackson 1993). Larger values of PC1 for both fins correspond with higher R:G and G:B values (Tables SD1-4, i.e., longer-wavelength colors).

To evaluate robustness of our results reported in the text, we (1) examined the Pearson correlations between the PC axes derived for *a** and *b** channels and those derived for R:G and G:B channels, and (2) tested the prediction that male body-color traits would be more exaggerated in low-predation blue holes by conducting univariate linear mixed models for each new PC axis with predation regime as our predictor variable, log-transformed lean weight as a covariate to control for body size, and population nested within predation regime included as random effect, as described in the Statistical Analyses.

Common-garden experiment

For the examination of male dorsal-fin color in the common-garden experiment, we reduced dimensionality of the proximal, middle and distal R:G and G:B values by conducting a PCA on the correlation matrix from which we retained the first two PC axes. Larger values of PC1

correspond to higher values of R:G and G:B measures. Larger values of PC2 correspond to higher R:G and lower G:B values (Table SD5).

We ran separate linear mixed-models with each PC axis as our response variable, predation regime, birth status (i.e., originally wild caught or lab born), and their interaction as main effects, log-transformed standard length (SL) as a covariate and population as a random intercept, as described in the Statistical Analyses. For the PC axes showing significant differences between predation regimes, we examined the Pearson correlation between PC axes calculated using the two different color spaces.

RESULTS

Our results reported in the main text were robust to the use of either human-specific or species-independent color metrics, as results using R:G and G:B color channels largely paralleled those for a^* and b^* color channels. First, PC axes derived from either a^* and b^* channels or from R:G and G:B channels were highly correlated with one another (average $r = 0.91$, all $P < 0.0001$), indicating strong similarities in the major axes of color variation captured by the two different types of color-space measurements. Second, dorsal- and anal-fin coloration quantified using R:G and G:B channels in wild-caught males photographed in the field significantly differed between low- and high-predation regimes (Table SD6). Dorsal- and anal-fin coloration was composed of longer wavelength colors in low-predation blue holes, in agreement with the results using $L^*a^*b^*$ color metrics.

Moreover, males originally derived from low-predation blue holes had significantly greater PC1 scores indicating longer wavelength dorsal-fin coloration (Table SD7). Furthermore, the degree of dorsal-fin coloration (PC1) did not significantly differ between males originally captured in the wild (and subsequently raised in the lab under common conditions for 8-13 months) and males born and raised in the lab (F1 or F2 generation) (Table SD7). There were no significant relationships found for PC2. PC1 calculated using a^* and b^* channels and PC1 calculated using R:G and G:B channels were highly correlated with one another ($r = 0.85$, $P < 0.0001$).

LITERATURE CITED

Endler, J. A. 2012. A framework for analyzing colour pattern geometry: adjacent colours. Biol. J. Linn. Soc. 107:233–253.

Frontier, S. 1976. Étude de la décroissance des valeurs propres dans une analyse en composantes principales: Comparaison avec le moddle du bâton brisé. J. Exp. Mar. Biol. Ecol. 25:67–75.

Jackson, D. A. 1993. Stopping rules in principal components analysis: a comparison of heuristical and statistical approaches. Ecology 74:2204–2214.

McKay, B. D. 2013. The use of digital photography in systematics. Biol. J. Linn. Soc. 110:1–13.

Table SD1. Principal components analysis of dorsal-fin R:G coloration of wild-caught *Gambusia hubbsi* males.

Measurement		PC1	PC2	PC3
Distal R:G	loadings	0.80	0.58	0.16
Middle R:G	loadings	0.90	-0.09	-0.42

Proximal R:G	loadings	0.85	-0.44	0.30
	% variance	72.56	17.97	9.47
	eigenvalue	2.18	0.54	0.28

Table SD2. Principal components analysis of dorsal-fin G:B coloration of wild-caught *Gambusia hubbsi* males.

Measurement		PC1	PC2	PC3
Distal G:B	loadings	0.77	0.64	-0.01
Middle G:B	loadings	0.88	-0.30	-0.37
Proximal G:B	loadings	0.88	-0.26	0.38
	% variance	71.98	18.66	9.37
	eigenvalue	2.16	0.56	0.28

Table SD3. Principal components analysis of anal-fin R:G coloration of wild-caught *Gambusia hubbsi* males.

Measurement		PC1	PC2
Distal R:G	loadings	0.98	-0.22
Middle R:G	loadings	0.98	0.22
	% variance	95.29	4.71
	eigenvalue	1.91	0.09

Table SD4. Principal components analysis of anal-fin G:B coloration of wild-caught *Gambusia hubbsi* males.

Measurement		PC1	PC2
Distal G:B	loadings	0.94	-0.34
Middle G:B	loadings	0.94	0.34
	% variance	88.3	11.7
	eigenvalue	1.76	0.23

Table SD5. Principal components analysis of dorsal-fin coloration of lab-reared *Gambusia hubbsi* males.

Measurement		PC1	PC2	PC3	PC4	PC5	PC6
Distal R:G	loadings	0.75	0.38	-.49	-.11	0.21	0.01
Distal G:B	loadings	0.82	-.23	-.46	-.1	-.22	0.03
Middle R:G	loadings	0.82	0.44	0.09	0.36	-.05	0.05
Middle G:B	loadings	0.89	-0.37	0.17	0.05	0.04	-0.21

Proximal R:G	loadings	0.63	0.50	0.53	-0.26	-0.06	0.01
Proximal G:B	loadings	0.72	-0.62	0.26	-0.01	0.1	0.16
	% variance	59.95	19.41	13.95	3.64	1.87	1.18
	eigenvalue	3.6	1.16	0.84	0.22	0.11	0.07

Table SD6. Summary of univariate general linear mixed models examining body color variation.

Trait	Term	*DF*	*F*	P^*
Dorsal fin R:G	log lean weight	1,97.82	11.78	<0.001
	predation regime	1,8.09	6.43	0.017
Dorsal fin G:B	log lean weight	1,98.08	14.76	0.002
	predation regime	1,8.1	5.54	0.023
Anal fin R:G	log lean weight	1,88.05	44.93	<0.001
	predation regime	1,8.1	6.55	0.017
Anal fin G:B	log lean weight	1,88.2	28.48	<0.001
	predation regime	1,8.1	4.91	0.029

Note: One-tailed *P* values shown.

Table SD7. Results from a linear mixed-model (treating population as a random effect) evaluating divergence in dorsal-fin color (PC1) of male *Gambusia hubbsi* from two high- and two low-predation blue holes from Andros Island, The Bahamas when kept or reared under common conditions in the lab (i.e., Birth Status).

Term	*DF*	*F*	*P*
SL	1,28.64	2.65	0.056
Birth Status	1,23.44	0.752	0.197
Predation Regime	1,1.99	8.549	0.05
Predation Regime x Birth Status	1,18.25	0.004	0.476

Note: One-tailed *P* values shown.

EVOLUTION OF MALE COLORATION DURING A POST-PLEISTOCENE RADIATION OF BAHAMAS MOSQUITOFISH (*GAMBUSIA HUBBSI*)

Ryan A. Martin[1,*], Rüdiger Riesch[2], Justa L. Heinen-Kay, and R. Brian Langerhans

SUPPLEMENTAL MATERIAL D: PRINCIPAL COMPONENTS ANALYSIS

Table SC1. Principal components analysis of dorsal-fin size of *Gambusia hubbsi* males.

Measurement		PC1	PC2
Dorsal-fin length	loadings	0.71	-0.70
Dorsal-fin height	loadings	0.71	0.70
	% variance	50.56	49.44
	eigenvalue	1.00	0.98

Table SC2. Principal components analysis of gonopodium size of *Gambusia hubbsi* males.

Measurement		PC1	PC2
gonopodium length	loadings	0.92	-0.37
gonopodium area	loadings	0.92	0.37
	% variance	86.1	13.9
	eigenvalue	1.72	0.27

Table SC3. Principal components analysis of caudal-fin size of *Gambusia hubbsi* males.

Measurement		PC1	PC2
Caudal-fin length	loadings	0.80	-0.58
Caudal-fin height	loadings	0.80	0.58
	% variance	65.26	34.74
	eigenvalue	1.30	0.69

Table SC4. Principal components analysis of blue-hole background habitat color.

Measurement		PC1	PC2
Habitat color *a**	loadings	0.78	-0.63
Habitat color *b**	loadings	0.78	0.63
	% variance	60.58	39.42
	eigenvalue	1.21	0.79

Table SC5. Principal components analysis of dorsal-fin *a** coloration of *Gambusia hubbsi* males.

Measurement		PC1	PC2	PC3
Distal *a**	loadings	0.71	-0.67	0.22
Middle *a**	loadings	0.91	0.04	-0.42
Proximal *a**	loadings	0.77	0.58	0.29
	% variance	63.70	26.10	10.17
	eigenvalue	1.90	0.78	0.31

Table SC6. Principal components analysis of dorsal-fin *b** coloration of *Gambusia hubbsi* males.

Measurement		PC1	PC2	PC3
Distal *b**	loadings	0.68	0.73	0.06
Middle *b**	loadings	0.86	-0.36	0.36
Proximal *b**	loadings	0.89	-0.21	-0.40
	% variance	66.80	23.60	9.68
	eigenvalue	2.00	0.71	0.29

Table SC7. Principal components analysis of anal-fin *a** coloration of *Gambusia hubbsi* males.

Measurement		PC1	PC2
Distal *a**	loadings	0.95	-0.30
Middle *a**	loadings	0.95	0.30
	% variance	91.17	8.83
	eigenvalue	1.82	0.18

Table SC8. Principal components analysis of anal-fin *b** coloration of *Gambusia hubbsi* males.

Measurement		PC1	PC2
Distal *a**	loadings	0.96	-0.27
Middle *a**	loadings	0.96	0.27
	% variance	92.67	7.33
	eigenvalue	1.85	0.15

Table SC9. Principal components analysis of dorsal-fin coloration of lab-reared *Gambusia hubbsi* males.

Measurement		PC1	PC2	PC3	PC4	PC5	PC6
Distal *a**	loadings	0.67	0.31	-0.65	-0.13	-0.11	-0.01
Distal *b**	loadings	0.79	-0.15	0.33	-0.45	-0.21	0.03
Middle *a**	loadings	0.61	0.66	0.13	-0.09	0.41	0.03
Middle *b**	loadings	0.88	-0.39	0.05	0.17	0.07	-0.18
Proximal *a**	loadings	0.37	0.79	0.21	0.34	-0.28	0.00
Proximal *b**	loadings	0.73	-0.60	-0.03	0.29	0.38	0.15
	% variance	48.26	28.07	10.00	7.57	5.14	0.01
	eigenvalue	2.90	1.68	0.60	0.45	0.31	.06